Semicond. Sci. Technol. **11** (1996) 289–299. Printed in the UK

Nonlinear photothermal modulated optical reflectance and photocurrent phenomena in crystalline semiconductors: I. Theoretical

Robert E Wagner and Andreas Mandelis

Photothermal and Optoelectronic Diagnostics Laboratory, Department of Mechanical Engineering, University of Toronto, Toronto, Ontario M5S 1A4, Canada

Received 30 August 1995, accepted for publication 14 November 1995

Abstract. The effect of nonlinear carrier recombination on the photothermal modulated optical reflectance (PMOR) signal of a crystalline semiconductor has been theoretically modelled. The PMOR signal consists of both thermal and Drude (free-carrier) components, and nonlinear recombination influences it through its direct effect on the modulated carrier density, and its indirect effect on the modulated sample temperature. Quadratic recombination was shown to lead to a sublinear intensity dependence of the photocurrent amplitude at elevated optical excitation intensities; cubic recombination leads to a supralinear intensity dependence of the PMOR amplitude accompanied by a progressive phase lag dependence on pump laser-beam intensity. The effect of nonlinear carrier and heat-flux gradients was also considered and found to be negligible with PMOR detection.

1. Introduction

Photothermal modulated optical reflectance (PMOR) is a technique which probes the modulation of a sample's optical reflectance when the sample is excited with an intensity-modulated laser beam [1–3]. When the excitation intensity is high ($> 10^4$ W cm^{-2}), and when the probe wavelength is distant from any critical points in the density of states, it is normally assumed that the reflectance is modulated through a combined thermal and Drude (free-carrier) mechanism [1–3]. Therefore, in order to model the PMOR signal in a crystalline material, it is necessary to obtain expressions for the modulated sample temperature, ΔT, and the modulated free-carrier density, ΔN. The theoretical PMOR signal can be expressed as the modulated reflectance, ΔR

$$\Delta R = \frac{\partial R}{\partial T}\Delta T + \frac{\partial R}{\partial N}\Delta N \tag{1}$$

where $\partial R/\partial T$ is the temperature reflectance coefficient and $\partial R/\partial N$ is the Drude reflectance coefficient.

ΔN is obtained by solving the carrier diffusion equation and ΔT is obtained by solving the heat diffusion equation. When linear diffusion equations are employed, ΔN and ΔT can be calculated quite readily, in both the one-dimensional limit and for the case where the exciting beam has a Gaussian profile with radial symmetry. In reality, the carrier and heat diffusion equations often have a significant degree of nonlinear character, especially when the pump power is large. In this work the effect of nonlinear carrier recombination upon ΔN and ΔT will be considered in the one-dimensional limit.

Forget *et al* [4] have already examined the effect of Auger recombination upon the PMOR signal, but their analysis was only approximate. For instance, instead of solving for N_1 and N_2, the d.c. and fundamental a.c. components of the photocarrier density, they only examined the time-independent form of the carrier transport equation. Also, they employed certain approximations, such as the assumption of surface-localized excitation, which are not valid under all conditions. Cheng *et al* [5] also included Auger recombination in their model of the nonlinear piezoelectric photoacoustic effect for semiconductors with an applied d.c. electric field, but they only solved the carrier transport equation in the 'subsurface approximation' limit. For this approximation, the carrier transport equation was linearized by making the assumption that only the surface value of the carrier diffusion length is significant in determining the surface value of the modulated carrier density; thus, the problem was reduced to solving a pair of linear differential equations and a pair of nonlinear algebraic equations. The subsurface approximation appears to be useful for finding the surface value of the carrier density, but it is quite limiting when one is calculating the recombination heating term in the heat diffusion equation; in order to derive the recombination heating term one

 © 1996 IOP Publishing Ltd

must accurately know the modulated carrier density over at least one thermal diffusion length, which can be quite large at lower modulation frequencies. In the present case, a rigorous, generalized multiharmonic analysis is performed and the results are tested using numerical finite difference methods. The insights thus gained on the various nonlinearities in the PMOR signal can be used to elucidate the quantitative analysis of experimental PMOR data.

2. The Drude or free-carrier component of ΔR

2.1. Special case: optical excitation of transparent semiconductors

In order to characterize the effect of nonlinear recombination upon the modulated carrier density, the following form of the carrier diffusion equation will be examined:

$$\frac{\partial N}{\partial t} = D\frac{\partial^2 N}{\partial x^2} - g_1(N-N_0) - g_2(N-N_0)^2 - g_3(N-N_0)^3 + S(x)(1+\mathrm{e}^{\mathrm{i}\omega t}). \tag{2}$$

Here, N represents either the free-electron density (n), or the hole density (p), and N_0 is the equilibrium carrier density. Also, D is the average carrier diffusion coefficient for electrons and holes; this average value represents an attempt to account for the Dember effect [6], and is used in place of the more complicated ambipolar relation [7]. g_1 is the monomolecular (linear) carrier recombination coefficient, and is the inverse of the linear carrier lifetime, τ. g_2 is the bimolecular (quadratic) carrier recombination coefficient, and is usually associated with band-to-band radiative recombination. g_3 is the Auger (cubic) carrier recombination coefficient. The three recombination modes considered above have been examined in detail by Blakemore [8]. In truth, it is not always possible to have separate terms for the three recombination effects represented in equation (2), but this approximation is valid for the high-level optical injection conditions which are present with the use of tightly focused laser excitation [9]. In equation (2), $S(x)$ is the volume number density of carriers generated per unit time, and $f(t) = 1 + \mathrm{e}^{\mathrm{i}\omega t}$ is the temporal modulation function of the excitation beam.

Another approximation related to equation (2) is that the temperature gradients induced in the sample have no influence upon carrier transport. The validity of this assumption is not readily obvious; therefore, the appendix examines the issue and confirms this hypothesis.

In most PMOR experiments the free carriers are generated by a sinusoidal source. Thus, in equation (2) the carrier density can be expressed as

$$N(x,t) = N_0 + \sum_{m=1}^{\infty} N_m(x)\mathrm{e}^{\mathrm{i}\omega(m-1)t}. \tag{3}$$

When equation (3) is substituted into equation (2) it is found that each harmonic ($\mathrm{e}^{\mathrm{i}\omega m t}$) is associated with a separate nonlinear differential equation: the differential equation for the d.c. component of $N(x)$ is found by collecting terms which have no time dependence:

$$D\frac{\mathrm{d}^2 N_1}{\mathrm{d}x^2} - g_1 N_1 - g_2 N_1^2 - g_3 N_1^3 = -S(x). \tag{4}$$

The first-harmonic component N_2 is found by equating coefficients of the $\mathrm{e}^{\mathrm{i}\omega t}$ factor:

$$D\frac{\mathrm{d}^2 N_2}{\mathrm{d}x^2} - \mathrm{i}\omega N_2 - g_1 N_2 - 2g_2 N_1 N_2 - 3g_3 N_1^2 N_2 = -S(x) \tag{5}$$

where it should be apparent that N_2 is dependent on the d.c. component N_1. In general, the determination of the first-harmonic component is quite complex because two nonlinear differential equations must be solved. Equations (4) and (5) can be easily examined in order to identify approximate trends, which later can be compared with exact numerical solutions.

With regard to equation (4), this equation can be approximated as linear under 'low' excitation conditions, $N_1 \ll g_1/g_2$ and $N_1 \ll (g_1/g_3)^{1/2}$; in this case, N_1 is small, and the $g_1 N_1$ recombination term is dominant. The linear limit of equation (4) is

$$D\frac{\mathrm{d}^2 N_1}{\mathrm{d}x^2} - g_1 N_1 = -S(x). \tag{6}$$

In order to obtain a simple approximate but analytic solution for comparative purposes, $S(x)$ in equation (6) will be considered to be a slowly varying function of x; this would occur if the optical absorption coefficient in the sample is small. In this case, diffusion effects are not significant and equation (6) can be solved analytically

$$N_1(x) = \frac{S(x)}{g_1} \tag{7}$$

where surface recombination has been neglected. Although ignoring diffusion effects is not very realistic in many cases, equation (7) illustrates a generally applicable result: $N_1(x)$ is linearly proportional to the pump intensity when recombination is linear.

Under 'moderate' excitation conditions, $g_1/g_2 \ll N_1 \ll g_2/g_3$ and $g_2 > (g_1 g_3)^{1/2}$, the $g_2 N_1^2$ recombination term in equation (4) may become dominant, and the relevant differential equation to be solved is nonlinear:

$$D\frac{\mathrm{d}^2 N_1}{\mathrm{d}x^2} - g_2 N_1^2 = -S(x). \tag{8}$$

If diffusion effects are again ignored, an approximate analytical solution for equation (8) is possible:

$$N_1(x) = \left(\frac{S(x)}{g_2}\right)^{1/2}. \tag{9}$$

Thus, $N_1(x)$ should be approximately proportional to the square root of the pump intensity when quadratic (bimolecular) recombination is dominant, and diffusion is negligible.

Finally, under 'high' excitation conditions, $N_1 \gg g_2/g_3$ and $N_1 \gg (g_1/g_3)^{1/2}$, the $g_3 N_1^3$ recombination term is expected to dominate, resulting in the following form of equation (4):

$$D\frac{\mathrm{d}^2 N_1}{\mathrm{d}x^2} - g_3 N_1^3 = -S(x). \tag{10}$$

Again ignoring diffusion effects

$$N_1(x) = \left(\frac{S(x)}{g_3}\right)^{1/3}. \quad (11)$$

Equation (11) illustrates that $N_1(x)$ should be approximately proportional to the cube root of the pump intensity when cubic or Auger recombination is dominant, and diffusion is minor.

It is also possible to examine the behaviour of $N_2(x)$, the first-harmonic component of $N(x)$, under similar conditions. Before any exact solutions for $N_2(x)$ are examined, it should be noted that under low excitation conditions, equation (5) reduces to

$$D\frac{d^2 N_2}{dx^2} - i\omega N_2 - g_1 N_2 = -S(x) \quad (12)$$

where linear recombination is assumed to dominate. This type of linear diffusion equation is often used in PMOR modelling because its 3D analogue can be solved routinely with a moderate amount of computer power. Various approximate solutions of equation (5) will be examined in order to generate a set of criteria which can be used to establish whether equation (12) is valid under given experimental conditions. In what follows, carrier diffusion will be ignored, which is strictly true with optical excitation of transparent semiconductors, usually in the subbandgap region. Then, the value for N_1 is given by equation (7); substituting this solution into equation (5) yields

$$-i\omega N_2 - g_1 N_2 - \frac{2g_2}{g_1}S(x)N_2 - \frac{3g_3}{g_1^2}S(x)^2 N_2 = -S(x). \quad (13)$$

Thus, $N_2(x)$ can be easily obtained

$$N_2(x) = \frac{S(x)}{g_1 + i\omega + (2g_2/g_1)S(x) + (3g_3/g_1^2)S(x)^2}. \quad (14)$$

If $S(x)$ is in the *low pump-intensity range*, $S(x) \ll g_1^2/2g_2$ and $S(x) \ll (g_1^3/3g_3)^{1/2}$, then it can be shown quite readily that equation (14) reduces to

$$N_2(x) = \frac{S(x)}{g_1 + i\omega}. \quad (15)$$

Therefore, $N_2(x)$ is linearly proportional to the pump intensity when recombination is linear.

At *moderate pump-intensity levels*, the value for $N_1(x)$ may be given by equation (9); substituting this solution into equation (5) yields

$$N_2(x) = \frac{S(x)}{g_1 + i\omega + 2g_2^{1/2}S(x)^{1/2} + (3g_3/g_2)S(x)}. \quad (16)$$

If $S(x)$ is in the 'moderate' range, $g_1^2/4g_2 \ll S(x) \ll 4g_2^3/9g_3^2$ and $g_2 > (3g_1g_3/4)^{1/2}$, then equation (16) simplifies to

$$N_2(x) = \frac{1}{2}\left(\frac{S(x)}{g_2}\right)^{1/2} \quad (17)$$

which indicates that the first harmonic of the free-carrier density should be proportional to the square root of the pump intensity when bimolecular recombination is dominant.

Finally, at the *highest pump-intensity levels*, the value for $N_1(x)$ is given by equation (11); substituting this solution into equation (5) yields

$$N_2(x) = \frac{S(x)}{g_1 + i\omega + (2g_2/g_3^{1/3})S(x)^{1/3} + 3g_3^{1/3}S(x)^{2/3}}. \quad (18)$$

In the 'high' excitation range, $S(x) \gg (g_1^3/27g_3)^{1/2}$ and $S(x) \gg 8g_2^3/27g_3^2$, the dominant term in the denominator of equation (18) is the Auger term, so equation (18) can be approximated by

$$N_2(x) = \frac{1}{3}\left(\frac{S(x)}{g_3}\right)^{1/3} \quad (19)$$

which indicates that $N_2(x)$ should be proportional to the cube root of the excitation intensity when carrier diffusion is negligible.

From the preceding analysis of the carrier diffusion equation, one important conclusion can be made. If a PMOR signal is composed mainly of a free-carrier component, then the validity of using equation (12) instead of equation (5) to model the effect can be tested by examining the linearity of the PMOR signal: if it has a noticeable sublinear intensity dependence, nonlinear recombination effects may be important, and a more complicated diffusion equation than equation (12) must be solved.

2.2. General case: exact finite-difference treatment

Unfortunately, the above treatment is only valid in the special case when carrier diffusion is negligible, which is only true when the optical absorption length L_α is greater than the carrier diffusion length L_D. In most PMOR experiments the sample is excited with strongly absorbed light for which the optical absorption coefficient α (or $1/L_\alpha$) is greater than 10^6 m^{-1}, or L_α is less than 1 μm. Since L_D in crystalline silicon is on the order of 100 μm, clearly L_α is usually much smaller than L_D under conditions of super-bandgap optical excitation. To study the effects of carrier diffusion on the solution of equations (4) and (5), these equations can be rigorously solved for typical experimental situations using a finite difference technique.

For the finite difference solution, the sample of thickness L was divided into n layers, each of thickness $\Delta x = L/n$. Assuming linear optical absorption, the number of carriers generated in layer i was

$$G(i) = I\{\exp[-\alpha\Delta x(i-1)] - \exp(-\alpha\Delta x i)\} \quad (20)$$

where I (in m^{-2} s^{-1}) is the flux of super-bandgap photons entering the sample. Considering the conservation of carrier density for each layer in the sample, finite difference equations were obtained for the d.c. carrier density N_1 (one equation for each layer in the sample). With regard to the finite difference equations for the first-harmonic component N_2, the solution for N_2 is real when $\omega \ll 1/\tau$, that is, at low modulation frequencies. Since this limit is experimentally

common and theoretically convenient, it will be considered here. In this case the finite difference equations for N_2 are similar to those for N_1. The strategy for obtaining a numerical solution for $\{N_1(i)\}$ and $\{N_2(i)\}$ is to assume starting values for these quantities such as the analytical solution in the absence of nonlinear recombination, and then to iteratively obtain improved values for $\{N_1(i)\}$ and $\{N_2(i)\}$ until the solution converges. In the present case, the rate of solution convergence depends upon the value of Δx, or upon the number of layers n. For instance, when the sample thickness was assumed to equal $0.8L_D$ and n was set to 50, up to 12 000 iterations were required for the solution to converge. Convergence was assumed to occur when the fractional change of $\{N_1(i)\}$ and $\{N_2(i)\}$ was less than 10^{-6} between successive iterations. When n was increased to 500, convergence was orders of magnitude slower. Overall, for the simulations to be presented in this work, the sample thickness was always $0.8L_D$, and n ranged from 50 to 200. For these standard values of L and n, the value of Δx was about 3×10^{-6} m; thus, optical absorption profiles were not resolvable for absorption coefficients above 3×10^5 m^{-1} (or $1/\Delta x$).

2.3. Numerical simulations

In order to examine the effect of carrier diffusion on the intensity dependence of the free-carrier density, a number of simulations were carried out for silicon. Since the Drude component of the PMOR signal is sensitive to the surface value of the free-carrier density, $N_1(1)$ and $N_2(1)$ were determined as a function of I, under two conditions of opacity:

(i) Moderately high optical absorption coefficient, $\alpha = 10^4$ m^{-1}; thus, $L_\alpha \approx L_D$ and carrier diffusion is essentially suppressed. Two nonlinear special cases were considered: (a) linear and quadratic recombination present and (b) linear and cubic recombination present.

(ii) High optical absorption coefficient, $\alpha = 10^6$ m^{-1}; thus, $L_\alpha \ll L_D$ and carrier diffusion is significant. The same two special cases were examined as in (i).

Only two recombination modes were examined at a time, so that the transition from linear to nonlinear behaviour could be clearly observed. This avoids the situation where both quadratic and cubic recombination are significant over the same range of pump intensity. By judiciously choosing values of g_1, g_2 and g_3 it is possible to have ranges of intensity where only one recombination channel is dominant at a time, but in general, this is not the case.

One common experimental method for monitoring non-equilibrium free carriers in a semiconductor is to measure the sample photoconductivity using a transverse geometry [10]. If the applied electric field is uniform as a function of depth in the sample, then the photocurrent (PC) is proportional to the number of photocarriers integrated over the thickness of the sample. Thus, in addition to calculating $N_1(l)$ and $N_2(l)$ as outlined for the above simulations, the summed quantities

$$\sum N_1 \equiv \sum_{i=1}^{n} N_1(i) \tag{21a}$$

and

$$\sum N_2 \equiv \sum_{i=1}^{n} N_2(i) \tag{21b}$$

were also determined, as an approximation to the average photocarrier density integrated over the sample thickness. This makes possible a comparison between the intensity behaviour of the Drude component of the PMOR signal and the transverse photoconductivity. In all cases the carrier diffusion coefficient was 3×10^{-3} m^2 s^{-1} and the linear carrier lifetime was 10^{-5} s. The simulation diffusion coefficient is typical of high-quality silicon [11], and the value for the lifetime is about a factor of 10 below the maximum measured for silicon [11], and is typical of values obtained for silicon using the modulated photocurrent method [12]. Also, surface recombination velocities were set equal to zero, and the pump photon energy was 2.4 eV. In addition, $g_2 = 2\times10^{-19}$ m^3 s^{-1}, which ensures that quadratic recombination has a range of domination below the intensity range where cubic recombination dominates. According to Schroder [9], the value of g_2 for silicon and germanium at room temperature is about a factor of 10 lower than the value used in the present simulations. This does not alter the general characteristics of the simulations, but it does mean that higher pump powers are probably required to see nonlinear effects due to quadratic recombination in real Si or Ge. In fact, for Si and Ge it does not appear that there is any range in excitation power where quadratic recombination dominates over both linear and Auger recombination. The value of g_3 was set [4] equal to 4×10^{-43} m^6 s^{-1}.

Figure 1(a) shows $N_1(1)$ and $N_2(1)$ versus the absorbed optical intensity I (in W m^{-2}), when $\alpha = 10^4$ m^{-1} and both linear and quadratic recombination are present. At the lowest intensities, the data are linear, and $N_1(1) = N_2(1)$; in fact, linear behaviour was observed for all of the simulations at the lowest powers, and it indicates the dominance of the linear recombination mechanism. Then, as the intensity is increased, $N_2(1) < N_1(1)$, and $N_1(1) \to I^{0.56}$ and $N_2(1) \to I^{0.53}$. Note that this behaviour is very close to that predicted by equations (9) and (17), as expected.

Figure 1(b) shows $\sum N_1$ and $\sum N_2$ versus I, when $\alpha = 10^4$ m^{-1} and both linear and quadratic recombination are present. At the lowest intensities the data are linear, and $\sum N_1 = \sum N_2$. Then, as the intensity is increased, $\sum N_2 < \sum N_1$, and $\sum N_1 \to I^{0.53}$ and $\sum N_2 \to I^{0.50}$. Therefore, figures 1(a) and 1(b) indicate that when carrier diffusion is not significant, the surface carrier density and the integrated carrier density show a similar power dependence on the excitation intensity, at least when linear and quadratic recombination are present.

Figure 2(a) displays $N_1(1)$ and $N_2(1)$ versus I, when $\alpha = 10^6$ m^{-1} and both linear and quadratic recombination are present. As the intensity is increased, $N_1(1) \to I^{0.66}$ and $N_2(1) \to I^{0.65}$. This trend toward the two-thirds power-law behaviour was found to be a general result when the excitation is strongly localized at the surface, and quadratic recombination is dominant. In addition, figure 2(b) shows $\sum N_1$ and $\sum N_2$ versus I. At the higher intensities, $\sum N_1 \to I^{0.46}$ and $\sum N_2 \to I^{0.39}$. This

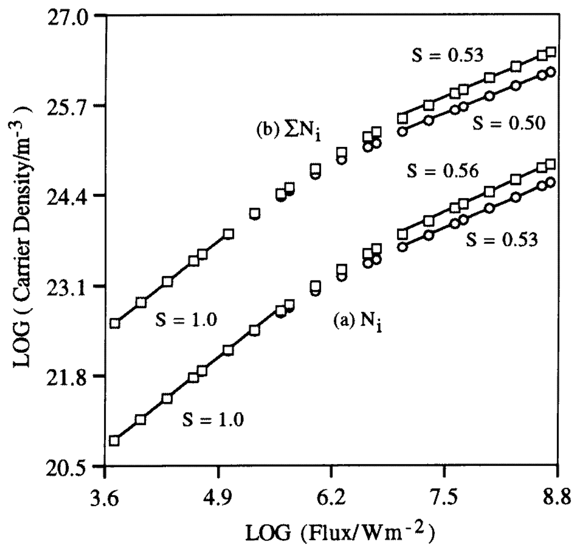

Figure 1. Theoretical simulation of carrier density (m^{-3}) versus absorbed optical flux (W m^{-2}) when both linear and quadratic recombination are present. The absorption coefficient is $\alpha = 10^4$ m^{-1}. (*a*) N_1 (□), N_2 (○); (*b*) $\sum N_1$ (□), $\sum N_2$ (○). The slopes of the linear sections are represented by the quantity *S*. See text for other simulation parameters.

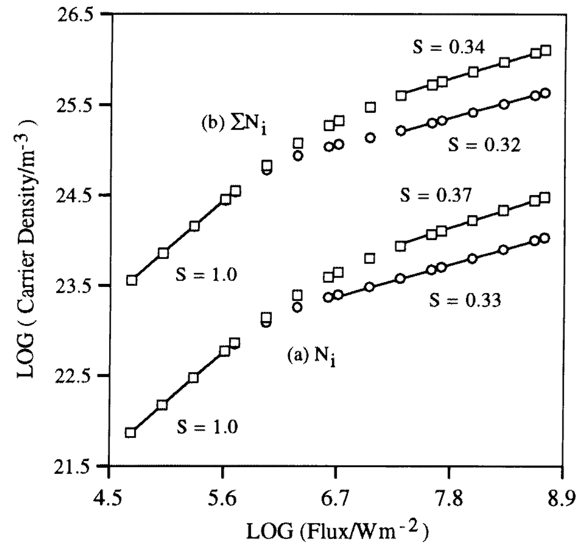

Figure 3. Theoretical simulation of carrier density (m^{-3}) versus absorbed optical flux (W m^{-2}) when both linear and Auger recombination are present. The absorption coefficient is $\alpha = 10^4$ m^{-1}. (*a*) N_1 (□), N_2 (○); (*b*) $\sum N_1$ (□), $\sum N_2$ (○). The slopes of the linear sections are represented by the quantity *S*. See text for other simulation parameters.

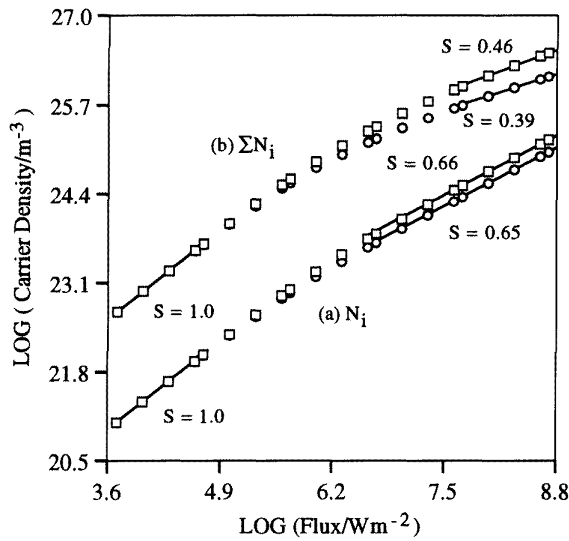

Figure 2. Theoretical simulation of carrier density (m^{-3}) versus absorbed optical flux (W m^{-2}) when both linear and quadratic recombination are present. The absorption coefficient is $\alpha = 10^6$ m^{-1}. (*a*) N_1 (□), N_2 (○); (*b*) $\sum N_1$ (□), $\sum N_2$ (○). The slopes of the linear sections are represented by the quantity *S*. See text for other simulation parameters.

result indicates that when carrier diffusion is significant, the surface carrier density and the integrated carrier density show a weaker dependence on the excitation intensity than when diffusion is neglected, at least when quadratic recombination is dominant. This is consistent with diffusive loss of carriers across the collection pathway.

In considering the situation where linear and cubic (Auger) recombination are present, figure 3(*a*) displays $N_1(1)$ and $N_2(1)$ versus I, when $\alpha = 10^4$ m^{-1}. As the intensity is increased, $N_1(1) \rightarrow I^{0.37}$ and $N_2(1) \rightarrow I^{0.33}$. These trends are consistent with the (limiting) equations (11) and (19), as expected. Furthermore, in figure 3(*b*), $\sum N_1 \rightarrow I^{0.34}$ and $\sum N_2 \rightarrow I^{0.32}$. Therefore, similar results to figures 1(*a*) and 1(*b*) are confirmed: when carrier diffusion is not significant, the surface carrier density and the integrated carrier density show a similar power dependence on the excitation intensity.

Figure 4(*a*) displays $N_1(1)$ and $N_2(1)$ versus I, when $\alpha = 10^6$ m^{-1} and both linear and cubic recombination are present. At the higher intensities, $N_1(1) \rightarrow I^{0.49}$ and $N_2(1) \rightarrow I^{0.48}$. This square-root power-law behaviour was found to be a general result when the excitation is strongly localized at the surface, and cubic recombination is dominant. Forget *et al* [4] have previously predicted a square-root dependence by obtaining an approximate analytical solution to the carrier diffusion equation (equation (5)) for a surface-localized source. The $\sum N_1$ and $\sum N_2$ versus I trends in figure 4(*b*) as the intensity is increased are $\sum N_1 \rightarrow I^{0.24}$ and $\sum N_2 \rightarrow I^{0.06}$. This result shows that when carrier diffusion is significant, the integrated carrier density exhibits a much weaker dependence on the excitation intensity than less opaque semiconductors, when nonlinear recombination is dominant. This is expected from the enhanced role of diffusion as a carrier-loss mechanism across the dark region behind the near-surface photoexcited volume.

3. The thermal component of ΔR

3.1. Theoretical and numerical

In order to determine the effect of nonlinear carrier recombination upon the modulated sample temperature, the

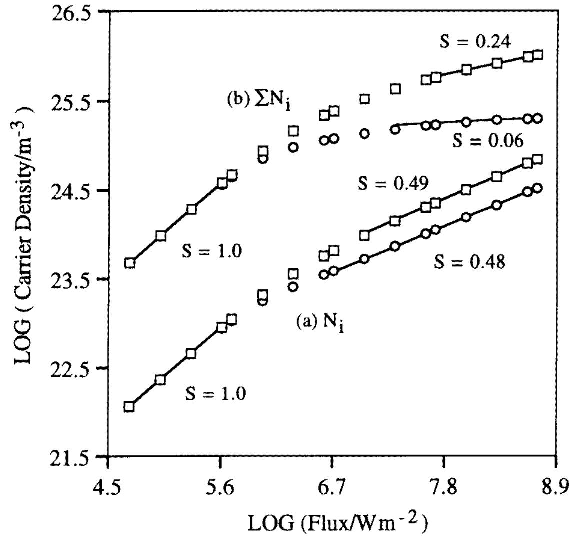

Figure 4. Theoretical simulation of carrier density (m^{-3}) versus absorbed optical flux ($W\ m^{-2}$) when both linear and Auger recombination are present. The absorption coefficient is $\alpha = 10^6\ m^{-1}$. (*a*) N_1 (□), N_2 (○); (*b*) $\sum N_1$ (□), $\sum N_2$ (○). The slopes of the linear sections are represented by the quantity S. See text for other simulation parameters.

following form of the heat diffusion equation was examined [13]:

$$\frac{\partial T}{\partial t} = \beta_s \frac{\partial^2 T}{\partial x^2} + \frac{E_g \beta_s}{k_s}[g_1(N - N_D) + g_2(N - N_0)^2 + g_3(N - N_0)^3] + \frac{(h\nu - E_g)\beta_s \alpha}{k_s} \exp(-\alpha x)(1 + e^{i\omega t}) \quad (22)$$

where T is the sample temperature, β_s is the sample thermal diffusivity, E_g is the energy gap, k_s is the sample thermal conductivity, $h\nu$ is the pump photon energy and α is the pump absorption coefficient. Two separate heating effects are included on the right-hand side of equation (22): the first term, which contains the free-carrier density N, represents the heat liberated when the photocarriers recombine non-radiatively. In the case of Si and Ge, the non-radiative quantum efficiency is assumed to be 1; this is not necessarily so for other, direct-gap semiconductors. Nevertheless, the photothermal modulated optical reflectance technique is only sensitive to the non-radiative component of carrier plasma and lattice de-excitation: in the case of radiative decay, a factor equal to the non-radiative quantum yield (≤ 1) would have to multiply each term in equation (22). The second term on the right-hand-side, which is proportional to $h\nu - E_g$, represents the heat released to the sample when the hot photocarriers are thermalized immediately after they are generated by the pump photons. Here, again, the non-radiative efficiency was assumed to be unity, or the term can be multiplied by the appropriate non-radiative quantum yield factor.

In the appendix, potential nonlinear gradient-originating heating terms are discussed. Since such terms are highly nonlinear, and are strongly coupled to the carrier diffusion equation, their consideration is crucial in determining the validity of the decoupling of carrier and thermal transport equations which is assumed in an *ad hoc* manner by most authors. The results of the appendix indicate that temperature-gradient and Thomson-effect nonlinearities are not central to PMOR studies using moderate optical pump fluences, such as in the present work. Therefore, substituting

$$T(x,t) = T_1(x) + T_2(x)e^{i\omega t} \quad (23)$$

and

$$N(x,t) = N_0 + N_1(x) + N_2(x)e^{i\omega t} \quad (24)$$

into equation (22) yields the following equation for T_2, the first-harmonic component of $T(x,t)$:

$$\frac{d^2 T_2}{dx^2} - i\frac{\omega}{\beta_s}T_2 = -\frac{E_g}{k_s}(g_1 N_2 + 2g_2 N_1 N_2 + 3g_3 N_1^2 N_2) - \frac{(h\nu - E_g)I\alpha}{k_s}\exp(-\alpha x). \quad (25)$$

Since the recombination heating term in equation (25) is nonlinear, this equation cannot be solved exactly by analytical means; instead, an approximate analytical solution was obtained as follows. First, $N_1(x)$ and $N_2(x)$ were obtained by the finite difference approach discussed in section 2. Then, these quantities were used to numerically obtain the recombination heating term on the right-hand side of equation (25), and this numerical solution was then fitted to a fourth-order polynomial function which was used to represent the recombination heating term in equation (25). The resulting equation to be solved was

$$a_1 + a_2 x + a_3 x^2 + a_4 x^3 + a_5 x^4 + E(x) = -\frac{E_g}{k_s}(g_1 N_2 + 2g_2 N_1 N_2 + 3g_3 N_1^2 N_2) \quad (26)$$

where

$$\frac{d^2 T_2}{dx^2} - i\frac{\omega}{\beta_s}T_2 = (a_1 + a_2 x + a_3 x^2 + a_4 x^3 + a_5 x^4) - \frac{(h\nu - E_g)I\alpha}{k_s}\exp(-\alpha x) \quad (27)$$

and $E(x)$ is the deviation between the fourth-order polynomial and the exact numerical function. In fact, when there was a sharp gradient in the carrier density near the sample surface, it was found that it was better to fit two separate polynomial functions to the recombination heating term, one near the sample surface and one for the remainder of the sample bulk. This two-curve fit was far superior to the fit which was obtained when only one polynomial function was employed over the whole sample depth. The only disadvantage to using the two-piece polynomial function is that the calculational complexity of the problem is increased, since two extra boundary conditions are required.

With regard to boundary conditions, it was assumed that both the front and back surfaces of the sample were carrier recombination sites:

$$\left[\frac{dT_2}{dx}\right]_{x=0} = \frac{-s_1 E_g}{k_s} N_2(1) \quad (28)$$

$$\left[\frac{dT_2}{dx}\right]_{x=L} = \frac{s_2 E_g}{k_s} N_2(n) \quad (29)$$

where s_1 and s_2 are the surface recombination velocities at $x = 0$ and $x = L$ respectively. In addition, when the two-curve polynomial fit was employed, both the temperature and its first derivative were required to be continuous at $x = L_p$. With regard to choosing the value for L_p by trial and error it was found that good results were obtained when $L_p = L/4$, where L is the sample thickness.

The effect of nonlinear recombination on the intensity dependence of the modulated sample temperature was tested by performing a number of numerical simulations. The electronic simulation parameters were identical to those used in section 2 with the Drude component of the PMOR signal, and they represent typical values for silicon [11]: $D = 3 \times 10^{-3}$ m^2 s^{-1}, $g_1 = 10^5$ s^{-1}, $E_g = 1.1$ eV and $h\nu = 2.4$ eV. With respect to the surface recombination velocity, it was found that varying this parameter did not alter the overall intensity dependence for a given sample. The thermal properties were those typical of silicon [11]: $\beta_s = 9.2 \times 10^{-5}$ m^2 s^{-1} and $k_s = 148$ W m^{-1} K^{-1}.

The first simulations were carried out with the following experimental parameters: linear and quadratic (or linear and cubic) recombination present, $\alpha = 10^4$ or 10^6 m^{-1}, and modulation frequency $f = 1$ kHz. Under these conditions it was found that the temperature modulation amplitude was a linear function of the pump intensity. This result was somewhat surprising, since N_2 showed strong sublinear behaviour over the same range of intensity. There are, however, two reasons for which nonlinear recombination does not affect the linearity of $T_2(0)$ for silicon at 1 kHz. First, a considerable portion of the sample heating, namely the carrier thermalization component, does not depend on the effects of nonlinear recombination. Second, the thermal diffusion length, $L_T = (2\beta/\omega)^{1/2}$, at 1 kHz is larger than the carrier diffusion length at all pump powers; therefore, the temperature modulation was only weakly dependent on the distribution of the recombination heating. Figure 5 shows a theoretical plot of the phase lag of $T_2(0)$ versus the pump intensity when both linear and quadratic recombination are present ($g_1 = 2 \times 10^{-19}$ m^3 s^{-1}), at 1 kHz; in this case, the variation of the phase lag with intensity is a clear indication that carrier recombination has become strongly nonlinear. As the intensity is increased, the effective carrier diffusion length is decreased, and more of the recombination heating occurs close to the surface where the carriers are generated; this leads to a decrease in the phase lag of the modulated surface heating. Figure 5 also indicates that when the absorption length is of the order of the carrier diffusion length (i.e. $\alpha = 10^4$ m^{-1}), which yields relatively weak carrier diffusion, the phase lag of $T_2(0)$ is less sensitive to nonlinear recombination than when the optical absorption length is much shorter.

Another simulation was carried out using the parameters listed above, but the modulation frequency was raised to 10 kHz, so the thermal diffusion length was somewhat less than both the sample thickness and the carrier diffusion length. Also, it was assumed that only linear and Auger recombination were present ($g_3 = 4 \times 10^{-43}$ m^6 s^{-1}). Figure 6(a) indicates that as the intensity is raised, $T_2(0)$ makes a transition from linearity to a weak supralinear power law ($I^{1.06}$). A second feature

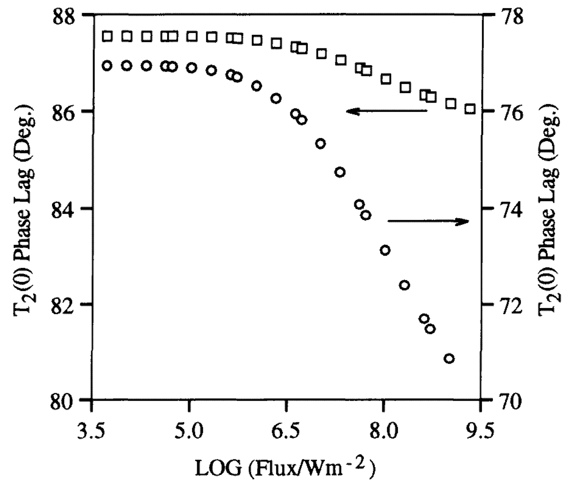

Figure 5. Theoretical simulation of the phase lag of $T_2(0)$ versus the absorbed optical flux (W m^{-2}) for c-Si (see text for material parameters). Both linear and quadratic recombination are present, and $f = 1$ kHz. The absorption coefficient is either (□) 10^4 or (○) 10^6 m^{-1}.

of figure 6(a) is that it also shows the intensity dependence of $T_2(0)$ under the assumption that $E_g = 2.4$ eV, so there is no thermalization heating and all of the sample heating is due to recombination. As the intensity is increased, the effective carrier lifetime decreases, where the effective lifetime under Auger recombination is based on equation (5): $\tau_{Auger} = g_3 N_1^2$. Eventually very little carrier diffusion occurs because the Auger lifetime is too short, and the recombination heating becomes very similar in spatial distribution to thermalization heating; thus, $T_2(0)$ becomes identical to that obtained when $E_g = 1.1$ eV, which is the actual situation for Si. In this limit, the increasingly surface-localized character of the non-radiative recombination becomes responsible for the observed supralinear power law.

Figure 6(b) shows the phase lag data corresponding to the amplitude data of figure 6(a). It gives further evidence that when Auger recombination is significant, the phase lag becomes smaller as the pump intensity is increased, because the heat generation distribution is moved closer to the sample surface. It should be emphasized that the phase changes are due to the lifetime-sensitive recombination heating effect.

The above simulations for $T_2(0)$ clearly indicate that even under the strongest nonlinear recombination conditions, the modulated surface temperature is only a weak supralinear function of the pump intensity, for one-dimensional diffusion. In addition, it can be stated that the supralinear effects are increased when the modulation frequency is increased, due to the decrease in the thermal diffusion length.

It can be mathematically shown that when carrier diffusion effects are weak, the recombination heating effect does not induce a significant nonlinearity in the dependence of $T_2(0)$ on I. From equation (25), the quadratic recombination heating term is proportional to $S_2 \equiv 2g_2 N_1 N_2$. When quadratic recombination is

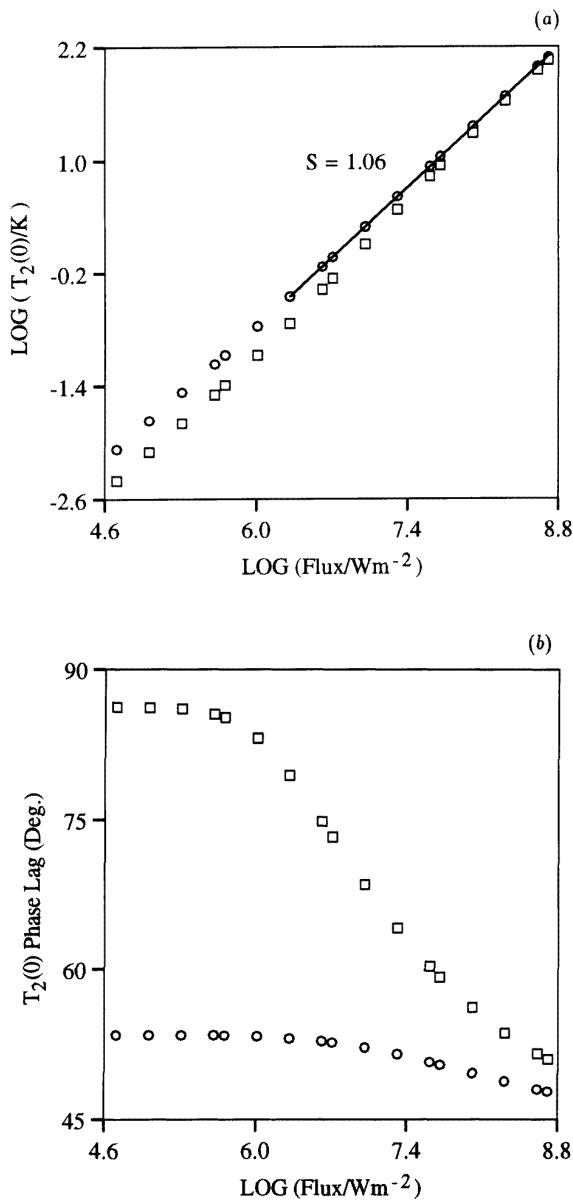

Figure 6. Theoretical simulation of (*a*) the amplitude and (*b*) phase lag of $T_2(0)$ versus the absorbed optical flux (W m^{-2}), for c-Si (see text for material parameters). Both linear and Auger recombination are present, f = 10 kHz and $\alpha = 10^6$ m^{-1}. The pump photon energy is 2.4 eV, and the energy gap is (○) 1.1 eV or (□) 2.4 eV. The slope of the linear section of the 1.1 eV curve is represented by the quantity S.

dominant, and under weak carrier diffusion conditions, $N_1 = (S(x)/g_2)^{1/2}$ (equation (9)) and $N_2 = (S(x)/g_2)^{1/2}/2$ (equation (17)). Thus, $S_2 = S(x)$, which is a linear function of the pump intensity. Likewise, the Auger recombination heating term is proportional to $S_3 \equiv 3g_3N_1^2/N_2$. When Auger recombination is dominant, in the zero carrier diffusion limit, $N_1 = (S(x)/g_3)^{1/3}$ (equation (11)), and $N_2 = (S(x)/g_3)^{1/3}/3$ (equation (19)). Thus, $S_3 = S(x)$. These analytical results indicate that even in the presence of strong nonlinear recombination, the modulated surface temperature should be a linear function of the pump intensity when carrier diffusion is weak, which occurs when the optical absorption length is longer than the carrier diffusion length. In order to isolate effects due to nonlinear recombination, carrier transport was assumed to be independent of the sample temperature; in fact, the present treatment can be readily altered to include the effect of sample temperature upon carrier transport [14].

4. Conclusions

The behaviour of the thermal/Drude PMOR effect has been modelled for the situation where carrier recombination is both linear and quadratic or cubic in the carrier density. The one-dimensional nonlinear carrier diffusion equation was solved using a finite-difference technique. The finite difference solution for ΔN is quite rigorous, and its only limitation is that one cannot resolve optical absorption when the absorption depth is less than Δx, the thickness of the discretized layers in the sample.

Using the same finite-difference approach, it was found that when nonlinear recombination dominates over linear recombination, the fundamental-frequency modulated carrier density at the surface, $N_2(1)$, has a sublinear dependence on the excitation intensity $I (N_2 \propto I^{\varepsilon}, \varepsilon < 1)$. The exponent ε was found to depend on several factors: on the nature of the recombination mechanism (quadratic or cubic) and on the importance, or not, of carrier diffusion. For example, when the optical absorption depth is greater than the carrier diffusion length, carrier diffusion is relatively weak and a larger value of ε is obtained than when the optical absorption length is much less than the carrier diffusion length, consistent with a diffusive carrier-loss mechanism.

The thermal component of the PMOR signal was also investigated by determining the modulated sample temperature in the presence of nonlinear recombination. The recombination heating term in the heat diffusion equation was represented by a two-curve fourth-degree polynomial function, allowing the one-dimensional heat diffusion equation to be solved analytically. The solution of the heat diffusion equation was not given explicitly, but it can be obtained in a straightforward manner. Simulations of the modulated surface temperature $T_2(0)$ indicated that even in the presence of strong nonlinear recombination, $T_2(0)$ should only have a weak supralinear dependence on the excitation power. On the other hand, the phase lag appears to be much more sensitive to the presence of nonlinear recombination. It is possible to stay within the linear recombination regime by utilizing a low excitation power, but even so, diagnostic tests must be carefully performed in order to confirm that linear recombination is indeed dominant.

Acknowledgments

The authors wish to acknowledge partial support of this project by the Natural Sciences and Engineering Research Council of Canada through a Collaborative Research Grant.

Appendix: Nonlinear gradient-originating effects on the decoupling of the carrier and heat diffusion equations

The various effects which may potentially contribute to the nonlinear intensity dependence of the PMOR signal, besides nonlinear carrier recombination, can be obtained by examining the equations normally used to model the modulated temperature and carrier density. In general, four coupled partial differential equations must be solved simultaneously to determine the modulated temperature and carrier density: the electron and hole diffusion equations, the Poisson equation, and the heat diffusion equation [14, 15].

The 1D hole diffusion equation is

$$\frac{\partial p}{\partial t} = \frac{-(p - p_0)}{\tau} + S(x,t) - \frac{\nabla \cdot J_h}{e} \tag{A.1}$$

where p is the hole density, p_0 is the equilibrium hole density, $S(x,t)$ is the generation term and J_h is the hole current density. Likewise, the 1D electron diffusion equation is

$$\frac{\partial n}{\partial t} = \frac{-(n - n_0)}{\tau} + S(x,t) + \frac{\nabla \cdot J_e}{e} \tag{A.2}$$

where n is the electron density, n_0 is the equilibrium electron density and J_e is the electron current density.

The current densities are given by

$$J_h = e\mu_h p\xi - eD_h\frac{\partial p}{\partial x} - r_h p\frac{\partial T}{\partial x} \tag{A.3}$$

and

$$J_e = e\mu_e n\xi + eD_e\frac{\partial n}{\partial x} - r_e n\frac{\partial T}{\partial x} \tag{A.4}$$

where ξ is the electric field and r_h and r_e are [14]:

$$r_h = \mu_h\left(eQ_h + \frac{\partial E_g}{\partial T}\right) \tag{A.5}$$

and

$$r_e = \mu_e\left(eQ_e - \frac{\partial E_g}{\partial T}\right) \tag{A.6}$$

where Q_h is the hole thermopower and Q_e is the electron thermopower.

Finally, the Poisson equation is

$$\frac{\partial \xi}{\partial x} = \frac{p(x) - n(x)}{\varepsilon\varepsilon_0}. \tag{A.7}$$

The following assumptions were made in order to obtain equations (A.1), (A.2) and (A.7):

(i) No carrier trapping occurs, so the electrons and holes have the same lifetime τ.

(ii) Electrons and holes are generated at the same rate $S(x,t)$, which is reasonable for band-to-band optical excitation.

(iii) In equation (A.7), trapped immobile charges were neglected.

In order to estimate the relative importance of the various terms which comprise $\nabla \cdot J_h$ in equation (A.1) and $\nabla \cdot J_e$ in equation (A.2), the following carrier/heat diffusion problem will be modelled. A semiconductor is illuminated with a modulated, strongly absorbed, uniform beam of light. There are no externally applied electric fields and no built-in electric field at the surface; $D_e = D_h = D$, so no Dember field is created. The carrier lifetime is constant. Finally, the carriers are assumed to be generated via a localized surface source, and the sample heating also occurs via a localized surface source.

Since the pump beam is modulated at an angular frequency ω, let

$$p(x) = p_0 + p_1(x) + p_2(x)e^{i\omega t} \tag{A.8}$$

$$n(x) = n_0 + n_1(x) + n_2(x)e^{i\omega t} \tag{A.9}$$

and

$$T(x,t) = T_1(x) + T_2(x)e^{i\omega t}. \tag{A.10}$$

Under these assumptions, it is possible to evaluate the $\nabla \cdot J$ terms of equations (A.1) and (A.2). Employing equations (A.3) and (A.4) it can be shown that when the field ξ is zero

$$\nabla \cdot J_h = -eD\frac{\partial^2 p}{\partial x^2} - r_h\frac{\partial p}{\partial x}\frac{\partial T}{\partial x} - r_h p\frac{\partial^2 T}{\partial x^2} \tag{A.11}$$

and

$$\nabla \cdot J_e = eD\frac{\partial^2 n}{\partial x^2} - r_e\frac{\partial n}{\partial x}\frac{\partial T}{\partial x} - r_e n\frac{\partial^2 T}{\partial x^2}. \tag{A.12}$$

If equations (A.9) and (A.10) are substituted into (A.12), the first harmonic component can be isolated:

$$(\nabla \cdot J_e)_\omega = eD\frac{\partial^2 n_2}{\partial x^2} - r_e\frac{\partial n_1}{\partial x}\frac{\partial T_2}{\partial x} - r_e\frac{\partial n_2}{\partial x}\frac{\partial T_1}{\partial x} - r_e(n_0 + n_1)\frac{\partial^2 T_2}{\partial x^2} - r_e n_2\frac{\partial^2 T_1}{\partial x^2}. \tag{A.13}$$

Equation (A.13) contains two distinct components, one of which is independent of temperature gradients (termed D_1) and one related to temperature gradients (termed D_2). Using the standard solution to the 1D excess carrier diffusion equation [7]

$$\frac{\partial^2 n_2}{\partial x^2} - \left(\frac{1}{D\tau} + \frac{i\omega}{D}\right)n_2 = 0 \tag{A.14}$$

for n_2 in equation (A.9) under oscillatory surface photocarrier generation

$$n_2(x) = \frac{I_0}{2}(\tau/D)^{1/2}\exp[-x/(D\tau)^{1/2}] \tag{A.15}$$

it is possible to write an explicit relation for D_1 at $x = 0$:

$$D_1(x = 0) = e\frac{I_0}{2}\frac{1}{(D\tau)^{1/2}}. \tag{A.16}$$

Similarly, using the 1D heat diffusion equation under oscillatory surface heat generation of intensity I_0

$$\frac{\partial^2 T_2}{\partial x^2} - \left(\frac{i\omega}{\beta}\right)T_2 = 0 \tag{A.17}$$

with the solution

$$T_2(x) = \frac{h\nu I_0(1-\mathrm{i})}{4k}\left(\frac{2\beta}{\omega}\right)^{1/2}\exp[-(1+\mathrm{i})(\omega/2\beta)^{1/2}x] \quad (A.18)$$

it is possible to write an explicit relation for D_2 at $x = 0$, by use of equations (A.13), (A.16) and (A.18):

$$D_2(x=0) = \frac{-r_e h\nu I_0^2}{2k} \times \left\{\frac{1}{D} + \left[\frac{n_0}{I_0} + \frac{1}{2}\left(\frac{\tau}{D}\right)^{1/2}\right]\frac{1+\mathrm{i}}{2}\left(\frac{2\omega}{\beta}\right)^{1/2}\right\} \quad (A.19)$$

where I_0 is the photon flux impinging on the surface of the semiconductor. In order to compare D_1 and D_2, various material and experimental parameters must be known. For highly focused laser beams (radius $\sim$ a few μm), typical values of I_0 for Ge and Si are approximately 10^{27} s^{-1} m^{-2}. The values of r_e for Ge and Si can be obtained from the literature [11]. Finally, the values for n_0 and p_0 can be calculated from knowledge of the resistivity and mobility.

For typical low-resistivity Si and Ge, at a frequency of 100 Hz, it is found that $D_2 > D_1$; this means that near the sample surface, the temperature-gradient effect can be more important than the density-gradient effect in determining the transport of carriers in the sample. This result may complicate the analysis because, when the temperature-gradient effect is included in the carrier diffusion equation, the two equations become strongly coupled. Furthermore, the temperature-gradient effect contributes to the nonlinear intensity dependence of the photocarrier density.

In the PMOR case with superbandgap optical excitation, it is believed that nonlinear recombination plays a more prominent role in influencing the photocarrier density than carrier diffusion effects related to temperature gradients, and this seems to be borne out by the PC data [12]. When the PMOR signal is dominated by the temperature modulation component, neglecting the temperature-gradient effect in the carrier diffusion equation may not be as significant a problem. In experiments where the pump photon energy is much larger than the bandgap, only a fraction of the sample heating is influenced by the carrier diffusion behaviour. A method for attenuating the temperature-gradient phenomenon is to lower the pump intensity, since the temperature gradient effect grows quadratically with intensity. A second method for minimizing the temperature gradient effect is to decrease the absorption coefficient of the pump beam, since a weakly absorbed beam generates a weak temperature gradient.

There is another gradient-originating thermoelectric heat source in semiconductors, which is usually neglected, namely the Thomson effect. It arises with the evolution of heat as an electrical current traverses a temperature gradient in a material [16]. In order to estimate the significance of the Thomson effect in PMOR studies, expressions can be written for the various heat sources in a photoexcited semiconductor.

The *first heat source* is due to thermalization of hot electrons and hot holes. From equation (28), this heat source is

$$F_1(x,t) = \frac{\beta_s}{k_s}(h\nu - E_g)\alpha \mathrm{e}^{-\alpha x}\frac{I_0}{2}(1+\mathrm{e}^{\mathrm{i}\omega t}). \quad (A.20)$$

At the sample surface, the first-harmonic component of F_1 is

$$F_{1,\omega}(x=0) = \frac{\beta_s}{k_s}(h\nu - E_g)\alpha\frac{I_0}{2}. \quad (A.21)$$

The *second heat source* is due to band-to-band carrier recombination. Assuming a constant carrier lifetime τ, from equation (22) this heat source can be written as

$$F_2(x,t) = \frac{\beta_s}{k_s}E_g\frac{N(x,t)-N_0}{\tau}. \quad (A.22)$$

Substituting equation (A.9) into (A.22) yields

$$F_2(x,t) = \frac{\beta_s}{k_s}E_g\frac{n_1(x)+n_2(x)\mathrm{e}^{\mathrm{i}\omega t}}{\tau}. \quad (A.23)$$

At the sample surface, the first-harmonic component of F_2 is

$$F_{2,\omega}(x=0) = \frac{\beta_s}{k_s}E_g\frac{I_0}{2}\frac{1}{(D\tau)^{1/2}}. \quad (A.24)$$

Finally, the *third heat source* (the Thomson heat) can be written as [16]

$$F_3(x,t) = \frac{\beta_s}{k_s}\langle T\rangle\frac{\partial T}{\partial x}\left(\frac{\mathrm{d}Q_e}{\mathrm{d}T}J_e + \frac{\mathrm{d}Q_h}{\mathrm{d}T}J_h\right) \quad (A.25)$$

where the first term in the round brackets is associated with the electron current, and the second term is associated with the hole current. $\langle T\rangle$ denotes the average temperature of the sample. In a semiconductor with no externally applied fields, at open circuit, the total current density $J_e + J_h$ is approximately zero at all times, due to the Dember effect [8]. Therefore, $J_h \approx -J_e$, and equation (A.25) can be written as

$$F_3(x,t) = \frac{\beta_s}{k_s}\langle T\rangle\left(\frac{\mathrm{d}Q_e}{\mathrm{d}T} - \frac{\mathrm{d}Q_h}{\mathrm{d}T}\right)\frac{\partial T}{\partial x}J_e. \quad (A.26)$$

For simplicity, the following definition can be used:

$$f_3 \equiv \frac{\beta_s}{k_s}\langle T\rangle\left(\frac{\mathrm{d}Q_e}{\mathrm{d}T} - \frac{\mathrm{d}Q_h}{\mathrm{d}T}\right). \quad (A.27)$$

Thus

$$F_3(x,t) = f_3\frac{\partial T}{\partial x}J_e. \quad (A.28)$$

Substituting equation (A.4) into (A.28), with $\xi = 0$, yields

$$F_3(x,t) = f_3\frac{\partial T}{\partial x}\left(eD\frac{\partial n}{\partial x} - r_e n\frac{\partial T}{\partial x}\right). \quad (A.29)$$

Overall, using the carrier [7] and heat [4] flux boundary conditions at $x = 0$, the first harmonic of equation (A.29) can be shown to be

$$F_{3,\omega}(x=0) = f_3\frac{h\nu}{2k}I_0^2\left\{e - r_e\frac{h\nu}{2k}\left[\frac{3}{2}I_0\left(\frac{\tau}{D}\right)^{1/2} + 2n_0\right]\right\}. \quad (A.30)$$

When typical experimental parameters for Ge and Si are used to estimate the values of the three heating sources discussed above, it is found that the largest heating effect is due to hot-carrier thermalization, equation (A.21), as expected. Somewhat surprisingly, the Thomson component, equation (A.30), is found to be only two orders

of magnitude less than the thermalization component. The recombination source, equation (A.24), is about five orders of magnitude less than the thermalization effect. Therefore, it is unlikely that the Thomson effect is very important in PMOR detection, since the present simulations indicate that it is much smaller than the carrier thermalization effect. Since the Thomson effect grows as $\partial T/\partial x$ increases, it can be experimentally attenuated by decreasing the absorption coefficient of the pump beam.

References

[1] Smith W L, Rosencwaig A and Willenborg D L 1985 *Appl. Phys. Lett.* **47** 584
[2] Opsal J and Rosencwaig A 1985 *Appl. Phys. Lett.* **47** 498
[3] Opsal J, Taylor M W, Smith W L and Rosencwaig A 1987 *J. Appl. Phys.* **61** 240
[4] Forget B C, Fournier D and Gusev V E 1992 *Appl. Phys. Lett.* **61** 2341
[5] Cheng J C, Zhang S Y and Lu Y S 1990 *J. Appl. Phys.* **68** 3865
[6] Goldman S R, Kalikstein K and Kramer B 1978 *J. Appl. Phys.* **49** 2849
[7] Sze S M 1981 *Physics of Semiconductor Devices* 2nd edn (New York: Wiley) p 87
[8] Blakemore J S 1987 *Semiconductor Statistics* (New York: Dover)
[9] Schroder D K 1990 *Semiconductor Material and Device Characterization* (New York: Wiley) pp 360–3
[10] Sze S M 1981 *Physics of Semiconductor Devices* 2nd edn (New York: Wiley) p 52
[11] Neuberger M 1971 *Group IV Semiconducting Materials* (New York: Plenum)
[12] Wagner R E and Mandelis A 1996 *Semicond. Sci. Technol.* **11** 300
[13] Fournier D, Boccara C, Skumanich A and Amer N M 1986 *J. Appl. Phys.* **59** 787
[14] Gallant M I and van Driel H M 1982 *Phys. Rev.* B **26** 2133
[15] Fahrenbruch A L and Bube R H 1983 *Fundamentals of Solar Cells* (New York: Academic) p 73
[16] Callen H B 1960 *Thermodynamics* (New York: Wiley) p 300